



Gravity triboelectric nanogenerator for the steady harvesting of natural wind energy

Yuqi Wang^{a,b,1}, Xin Yu^{a,c,1}, Mengfei Yin^{a,b,1}, Jianlong Wang^{a,b}, Qi Gao^a, Yang Yu^{a,b},
Tinghai Cheng^{a,b,d,*}, Zhong Lin Wang^{a,d,e,*}

^a Beijing Institute of Nanoenergy and Nanosystems, Chinese Academy of Sciences, Beijing 101400, China

^b School of Mechatronic Engineering, Changchun University of Technology, Changchun, Jilin 130012, China

^c School of Electrical and Electronic Engineering, Changchun University of Technology, Changchun, Jilin 130012, China

^d CUSPEA Institute of Technology, Wenzhou, Zhejiang 325024, China

^e School of Materials Science and Engineering, Georgia Institute of Technology, Atlanta, GA 30332-0245, United States

ARTICLE INFO

Keywords:

Triboelectric nanogenerator
Gravity
Natural wind
Steady energy harvesting

ABSTRACT

Triboelectric nanogenerator (TENG), as a renewable energy harvesting technology, has been verified as an effective approach for converting mechanical energy into electric energy. In a natural environment, the unsteadiness of TENG energy harvesting restricts the application and development of TENG. From this perspective, a gravity triboelectric nanogenerator (G-TENG) is developed for the first time to convert natural wind energy into steady electric energy, achieving the steady harvesting of natural wind energy. The G-TENG mainly comprises an energy input module, energy storage module, and energy output module. Random wind energy is transmitted from the input module to the storage module and converted into gravitational potential energy. Steady electric energy is ultimately obtained from the output module. The standard deviation (I_{SD}) of the short-circuit current peaks is under $0.31 \mu\text{A}$. Additionally, the fluctuation degree (I_{FD}) of the short-circuit current peaks is defined to describe the steady output capability of TENG. I_{FD} of the G-TENG can reach 2.3%. A steady current is thus achieved by the G-TENG in a natural environment. This research provides essential guidance for the steady harvesting of natural energy by the TENG.

1. Introduction

Renewable green energy has been considered an effective solution to the growing global energy crisis [1,2]. Mainstream methods of power generation, such as the generation of wind energy and solar power, are subject to many restrictions relating to the requirements of specific environmental conditions [3,4]. A brand new technology for energy harvesting is therefore imperative in the contemporary world.

Triboelectric nanogenerator (TENG), as an efficient approach to harvest the energy from the environment, has received extensive attention [5–7]. TENG based on the combination of triboelectrification effect and electrostatic induction was first proposed by Wang's group in 2012 [8] and extensively converts mechanical energy existing in the environment into electric energy [9–12]. TENG has the characteristics of low cost, easy fabrication, and versatile choices of materials and structures [1,13] and is widely employed in multiple fields of harvesting

mechanical energy from the environment [14–17], such as in the harvesting of energy from vibrations [18,19], acoustic waves [20], human motion [21,22], wind [23], the motion of rain drops [24], and water flow [25], and peculiarly in blue energy harvesting [26,27]. In terms of improving the output performance of TENG in the field of harvesting mechanical energy, researchers have made breakthroughs for different modes of TENG, especially the mechanical mode.

Herein, mainstream mechanical modes include machinery frequency enhancement [28–30], intermittent energy harvesting [31,32], and mechanical regulation [33,34]. However, the steadiness of current is an important indicator of TENG output performance that cannot be overlooked and yet, the phenomenon of TENG output instability has not been well clarified. An unsteady output cannot drive electronic modules to operate normally and can even damage precision electronic devices. To achieve a steady output of TENG, controlling the rotor speed of the generating unit is a key element according to the fundamental theory of TENG [8].

* Corresponding authors at: Beijing Institute of Nanoenergy and Nanosystems, Chinese Academy of Sciences, Beijing 101400, China.

E-mail addresses: chengtinghai@binn.cas.cn (T. Cheng), zhong.wang@mse.gatech.edu (Z.L. Wang).

¹ These authors contributed equally to this work.

Nomenclature	
F	driving resistance force of the G-TENG
G	gravity of the mass block
F_1	bending force of the FEP film
F_q	electrostatic force acting between the FEP film and copper
M	mass of the mass block
L_{ab}	working length of the FEP film
F_N	the resultant force of F_1 and F_q
F_f	friction force acting between the FEP film and copper

Therefore, a gravity triboelectric nanogenerator (G-TENG) is developed in the present work. The G-TENG is mechanically designed to convert natural wind energy into gravitational potential energy that is then transformed into steady electric energy, ensuring the steadiness of short-circuit current. Experimental results demonstrate that the G-TENG can generate a maximum open-circuit voltage of 500 V, maximum short-circuit current of 15 μ A, and maximum transferred charge of 200 nC. Furthermore, the standard deviation (I_{SD}) and fluctuation degree (I_{FD}) are proposed to evaluate the degree of steady output and the performance of TENG. In the simulated natural environment, I_{SD} is under 0.31 μ A and I_{FD} is less than 2.3% and an almost steady current is thus achieved. In a natural wind environment, a commercial thermometer is powered by the G-TENG with the assistance of a bridge rectifier in one complete cycle. The present work provides significant guidance for TENG in terms of the steady harvesting of natural energy.

2. Results and discussion

2.1. Structural design and working principle

Fig. 1 shows a schematic diagram of gravity triboelectric nano-generator (G-TENG). The G-TENG comprises an energy input module, energy storage module, and energy output module. The energy input module comprises a wind scoop and driving unit, the energy storage module comprises a string and mass block, and a generation unit plays the role of the output module, as shown in Fig. 1a. The principle of mechanical transmission is shown in Fig. 1b. The driving unit comprises a worm gear, mechanical switch, crown gears, and gear-shifting unit. First, the wind scoop is connected to the worm gear through a coupling, and the worm gear is connected to a mechanical switch. The mechanical switch controls the meshing of the crown gears, while a shaft connects the crown gears and the gear-shifting unit. The speed of the rotor can be increased by connecting the generation unit and the gear-shifting unit. When the natural wind blows on the wind scoop, the worm gear transmits the mechanical energy. The mechanical switch and crown gears control the rise or fall of the mass block, which can store or release gravitational potential energy. Finally, the mass block drives the rotor in the generation unit to operate through the gear-shifting unit. To better describe the structure of the G-TENG, the overall structure of the G-TENG is depicted in Fig. 1c while the generation unit comprising the rotor and stator is depicted in Fig. 1d and e.

Fig. 2a shows the overall operation principle of the G-TENG under three states in one total cycle. When the natural wind blows on the wind scoop, the mass block is moved upward by the driving unit. Meanwhile, the rotor remains static owing to the one-way clutch, as illustrated in Fig. 2a(i). The mechanical switch is triggered when the mass block reaches its highest point (Fig. 2a(ii)). At the same time, the mass block starts moving downward (Fig. 2a(iii)) after getting rid of the shackles of

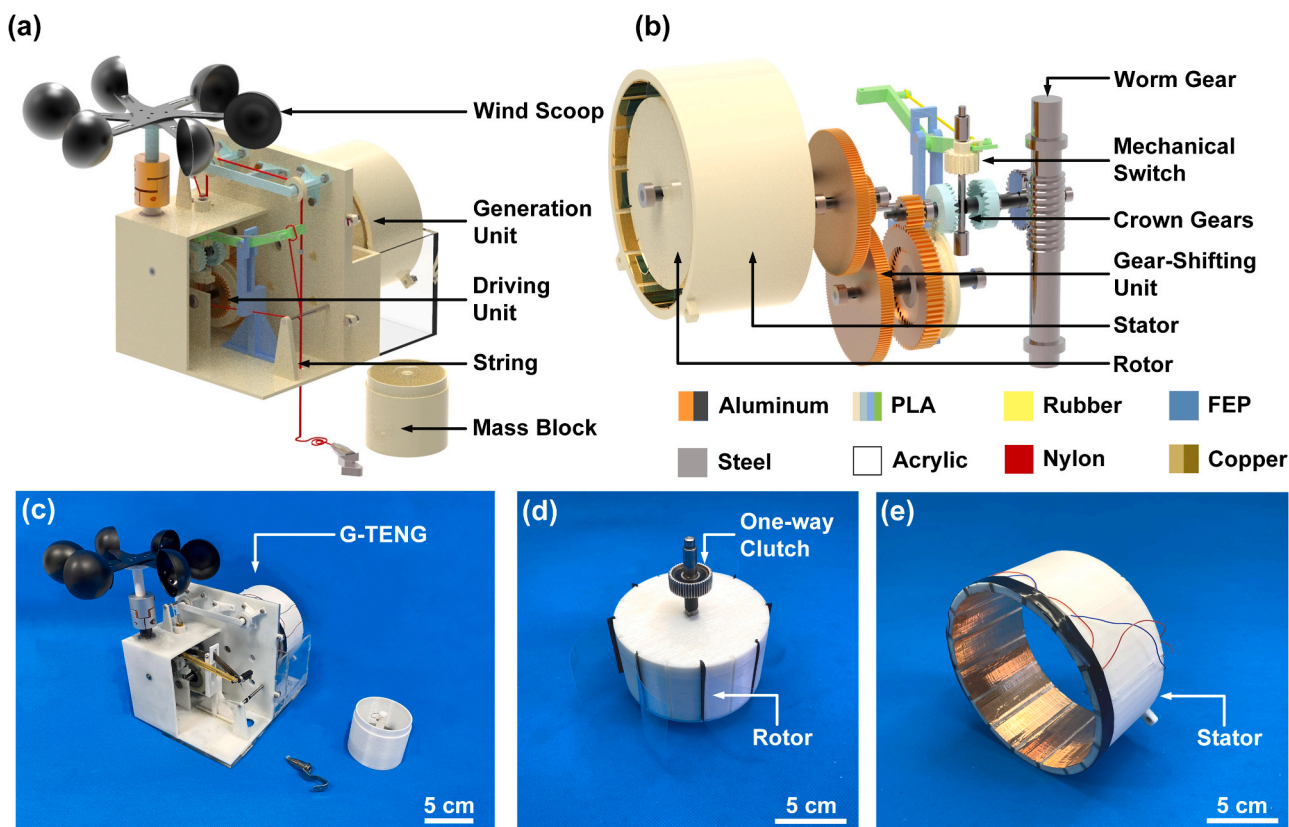


Fig. 1. Schematic diagrams of the gravity triboelectric nanogenerator (G-TENG): (a) schematic showing the overall structure of the G-TENG, (b) assembly relationship among mechanical components, and (c-e) photographs of the G-TENG, rotor, and stator.

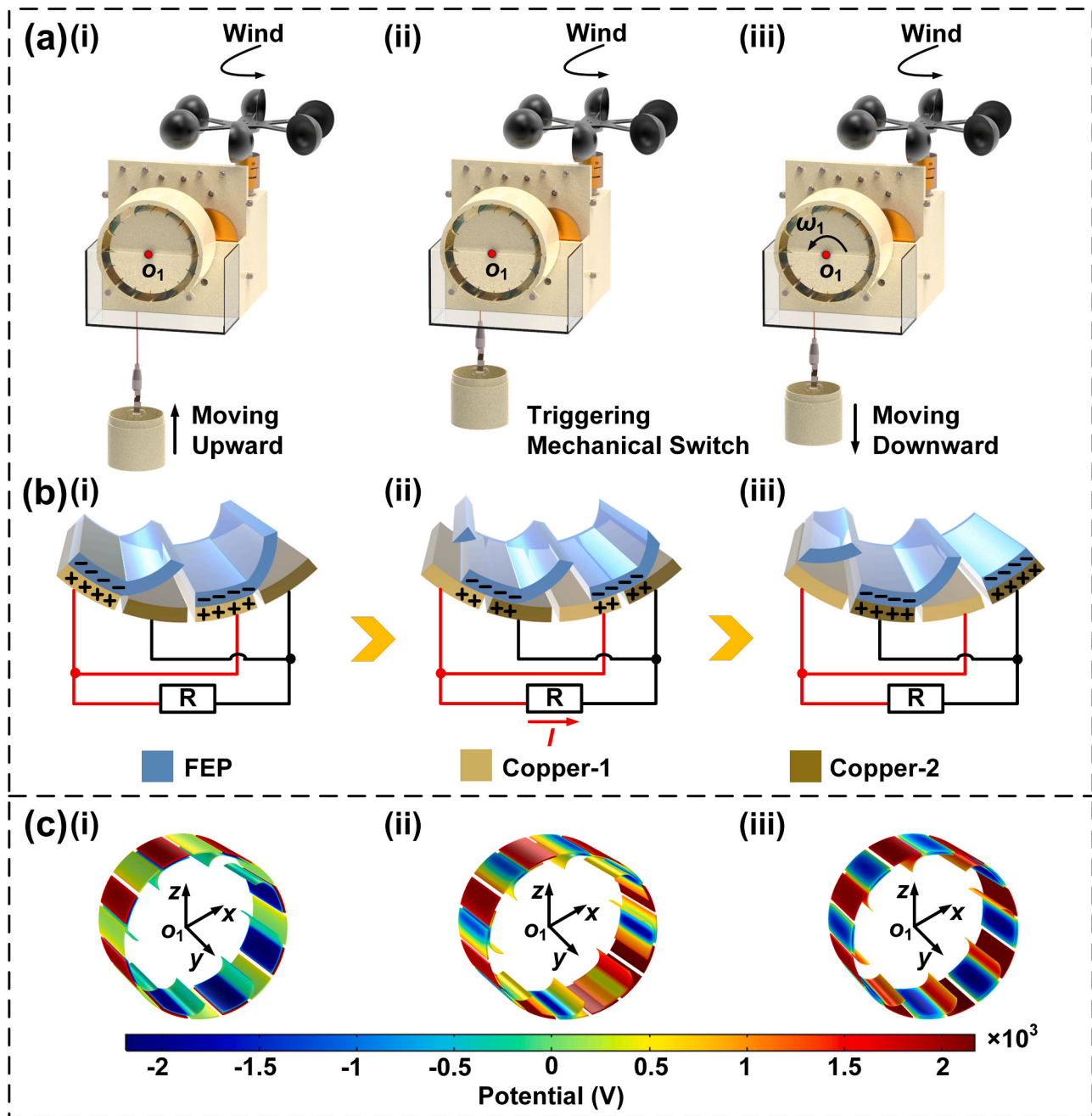


Fig. 2. Operating principle of the G-TENG: (a) operation mechanism of the G-TENG in three states for one total cycle, (b) schematics of the operation principle of the generation unit, and (c) 3D simulation results obtained using COMSOL and showing the working principle of the G-TENG at three positions.

the mechanical switch, and the rotor starts to rotate. The mechanical switch is triggered again when the mass block moves to its lowest point. At that moment, the cycle is complete and the next cycle starts. Specific details are shown in Fig. S1 (Supporting Information). The operation principle of the generation unit is depicted in Fig. 2b. The copper electrodes are connected alternately across the external circuit. In the original state, fluorinated ethylene propylene (FEP) films are in their initial position, and copper-1 and the FEP films generate equal quantities of opposite charges owing to the different electronegativities of the materials, as shown in Fig. 2b(i). With continued motion, the FEP films make contact with copper-2, as illustrated in Fig. 2b(ii). The positive charges are transferred from copper-1 to copper-2 across the external circuit through electrostatic induction. When the FEP films are in full contact with copper-2, all positive charges flow into copper-2, as depicted in Fig. 2b(iii). After the FEP films separate totally from copper-

2, the reversed current is produced and the next operation cycle begins. An alternating current is generated ultimately.

Furthermore, the 3D simulation results obtained using COMSOL are employed to elucidate the working principle in terms of the G-TENG to demonstrate the feasibility of the approach (see Fig. 2c).

2.2. Theoretical analysis

Fig. 3a shows the analysis of the force acting between the FEP film and copper in the generation unit when the G-TENG is running. The gravity of the mass block (G) can drive the G-TENG only when the mass of mass block (M) is large enough. The relationship among the forces acting between the copper and FEP film is shown in Fig. 3b. The bending force of the FEP film (F_1) is only relevant to the bending shape of the material. Meanwhile, the electrostatic force acting between the copper

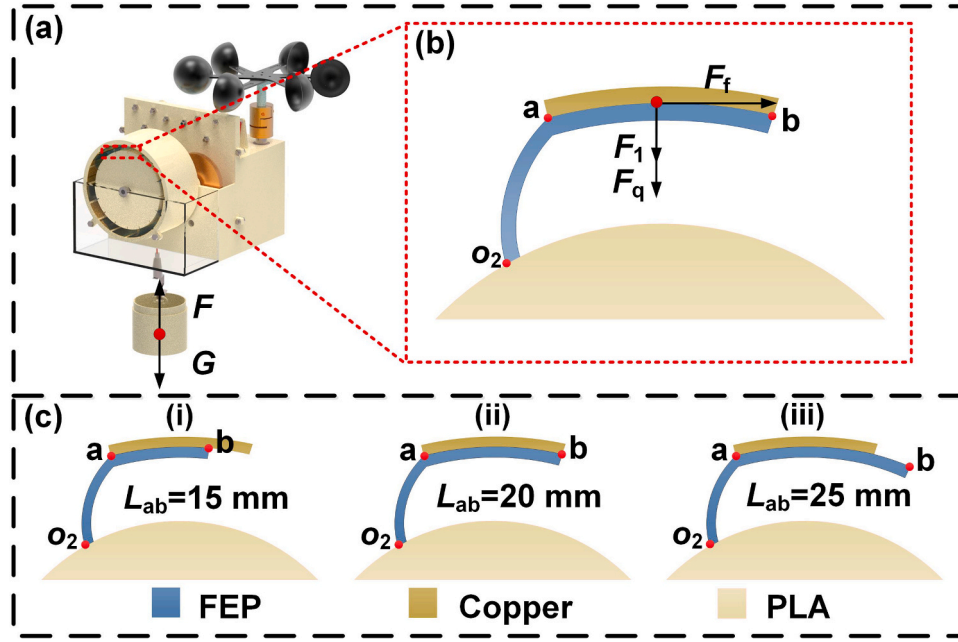


Fig. 3. Mechanical analysis of the G-TENG: (a) analysis of forces in the G-TENG, (b) analysis of forces acting between the FEP film and copper, and (c) contact states of the FEP film and copper for different L_{ab} .

and FEP film (F_q) is only relevant to the amount of charges on the surface of contact between the FEP film and copper. The values of F_1 and F_q affect the value of the friction force (F_f), and the friction force F_f is thus related to the working length of the FEP film (L_{ab}). Therefore, L_{ab} affects the minimum M of operation normally.

The relationship between L_{ab} and M is described in detail by the following equations. The force acting at the point of contact between the FEP film and copper is

$$F_N = F_1 + F_q, \quad (1)$$

where F_N is the resultant force of F_1 and F_q . The detailed derivation of F_q is given as Eqs. S1–S6 (Supporting Information). F_q is expressed as

$$F_q = \frac{\sigma Q_1}{\epsilon \epsilon_0}, \quad (2)$$

where σ is the surface charge density of the copper, Q_1 is the amount of charges on the surface of the copper and FEP film, ϵ is the permittivity of the FEP, and ϵ_0 is the vacuum dielectric constant. Therefore, F_q is proportional to Q_1 .

The G-TENG operates normally when the gravity of the mass block ($G = Mg$) is greater than or equal to F . When G is equal to F , it follows that

$$M \geq \frac{8\alpha\mu R_1 \left(F_1 + \frac{\sigma Q_1}{\epsilon \epsilon_0} \right)}{g r_1 \eta}, \quad (3)$$

where g is the coefficient of gravity and η is the mechanical efficiency. There is a positive correlation relationship between L_{ab} and Q_1 . Therefore, L_{ab} and M with a minimum driving mass have a positive relationship. The detailed derivation is given by Eqs. S7 and S8 and Fig. S2 (Supporting Information).

To investigate the relationship between L_{ab} and M , different lengths (15, 20, and 25 mm) are selected as shown in Fig. 3c.

2.3. Output performance

In terms of generating steady electric energy, L_{ab} and M —as important parameters of the G-TENG—are systematically investigated to

optimize the output performance of the G-TENG, as illustrated in Fig. 4. When L_{ab} is 15 mm, the short-circuit current, open-circuit voltage, and transferred charge of the G-TENG for different values of M are depicted in Fig. 4a (Supporting Information). In Fig. 4a, the output current peaks increase gradually with the augment of M . The insets show enlarged views of curves when M is 250 and 300 g. The output performances of the G-TENG are also investigated when L_{ab} is 20 and 25 mm, and the same with L_{ab} is 15 mm, as illustrated in Fig. 4b and c, and the Supplementary data are presented in Fig. S3 (Supporting Information). The short-circuit current depends on M owing to the relationship between G and F .

However, the fluctuation of the short-circuit current peaks affected by the operation of TENG cannot be ignored. The maximum of the short-circuit currents is denoted I_{max} , and all short-circuit current peaks from the first exceeding $0.9I_{max}$ to the last exceeding $0.9I_{max}$ are selected as measurement data (I_i). The standard deviation (I_{SD}) is expressed as

$$I_{SD} = \sqrt{\frac{\sum_{i=1}^n (I_i - I_{AVG})^2}{n}}, \quad (4)$$

where I_{AVG} is the average value of I_i , and n is the number of I_i . A detailed description is presented in Fig. S4 (Supporting Information).

To elucidate the effects of structural parameters on the output performance, I_{SD} of short-circuit current peaks of the G-TENG for different L_{ab} and M are investigated, as shown in Fig. 4d. The minimum driving masses corresponding to the three lengths are 250, 356, and 400 g. The corresponding I_{SD} of the short-circuit current peaks is minimal when M is 300, 406, and 450 g for different values of L_{ab} . F_q strongly affects the running of the rotor at low speed but hardly affects the running of the rotor at high speed. Therefore, when M is the minimum driving mass, I_{SD} is largest, and the short-circuit current peak changes periodically. As M increases, the effect of F_q on the rotor speed gradually decreases. There is an optimal M at which the rotor runs at almost uniform speed.

To objectively evaluate the steadiness of TENG, the fluctuation ratio of the short-circuit current peak (I_{FR}) is put forward as

$$I_{FR} = \frac{I_{SD}}{I_{AVG}}. \quad (5)$$

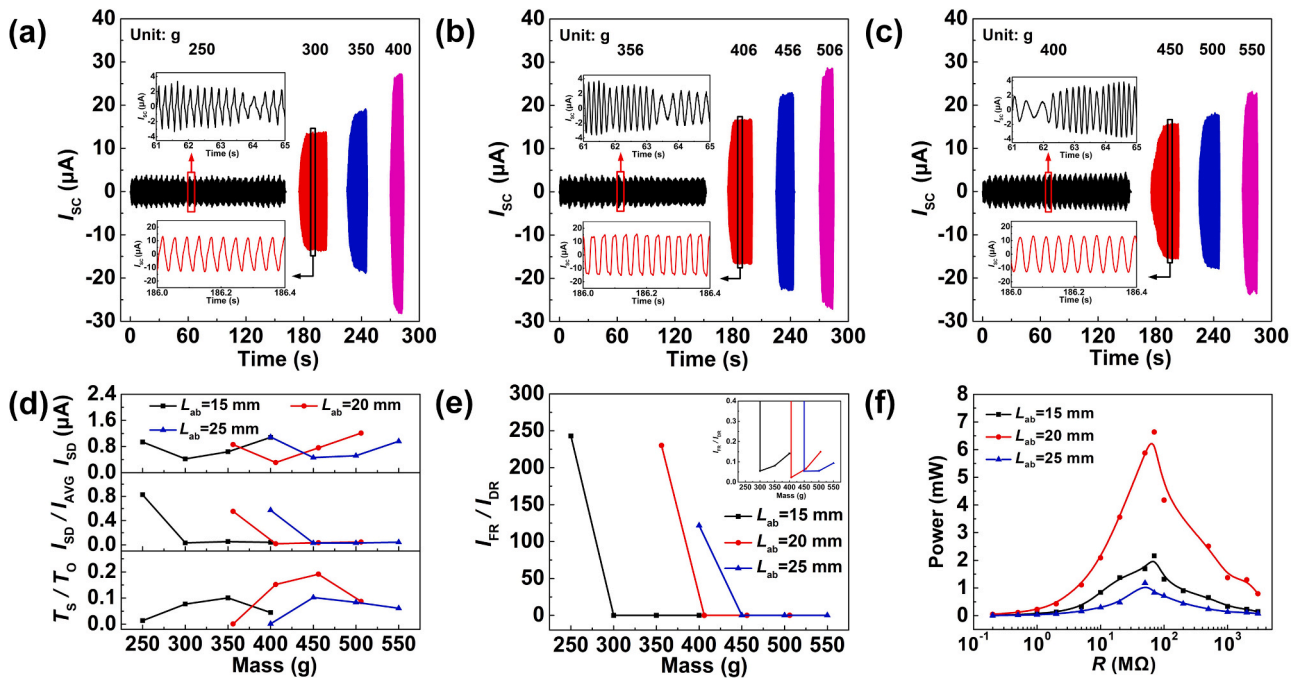


Fig. 4. Output performance of the G-TEG. (a–c) Short-circuit current peaks of the G-TEG when L_{ab} is 15, 20, and 25 mm. Insets show enlarged views of the short-circuit currents. (d) Standard deviations (I_{SD}), fluctuation ratio of the short-circuit current peaks (I_{FR}), and duty ratio of short-circuit current peaks (I_{DR}) for different L_{ab} . (e) Short-circuit current peak fluctuation degree (I_{FD}) for different L_{ab} . Insets show enlarged views of I_{FD} . (f) Peak power for different L_{ab} .

If T_S denotes the time for all short-circuit current peaks over $0.9I_{\max}$ and T_O denotes the time for the short-circuit current peak in the output stage, then the duty ratio of the steady current peak (I_{DR}) in one period is

$$I_{DR} = \frac{T_S}{T_O}. \quad (6)$$

Eqs. (5) and (6) reveal that a smaller value of I_{FR} and a larger value of I_{DR} correspond to better steadiness of TENG, as shown in Fig. 4d.

To more comprehensively evaluate the steadiness of the output when TENG is in an environment of random wind energy, the fluctuation degree (I_{FD}) of short-circuit current peaks in a complete generation cycle is proposed in this work as

$$I_{FD} = \frac{I_{FR}}{I_{DR}} \times 100\%. \quad (7)$$

A smaller value of I_{FD} means better capacity of the steady current, and I_{FD} for different values of L_{ab} and M is presented in Fig. 4e. The variation trends of I_{FD} and I_{SD} are consistent. M is 300 g (M_1), 406 g (M_2), and 450 g (M_3) when L_{ab} is 15 mm (L_{ab-1}), 20 mm (L_{ab-2}), and 25 mm (L_{ab-3}), respectively. Specific values are given in Table 1.

The running time for different values of L_{ab} and M is presented in Fig. S5 (Supporting Information). The peak power curves for different values of L_{ab} are shown in Fig. 4f. Because the FEP film and copper are completely aligned when L_{ab} is 20 mm, the output power is a maximum when L_{ab} is 20 mm. Therefore, the G-TEG has an optimal output when L_{ab} is 20 mm and M is 406 g.

The feasibility of the G-TEG generating steady current in a natural wind environment is demonstrated in the following experimental procedure. Fig. 5 shows the output performances of the G-TEG when L_{ab} is 20 mm and M is 406 g under different input conditions. Fig. 5a shows the overall experimental process and illustrates the energy conversion of

the G-TEG. First, a stepper motor provides input excitation to imitate rotation movement in different situations. The stepper motor is set in three working modes: uniform rotation, accelerated rotation, and random rotation. When the mechanical switch is on, random mechanical energy is input by the motor and stored as gravitational potential energy, and then the G-TEG steps into the energy storage stage. When the mechanical switch is off, the G-TEG steps into the energy release stage, and the gravitational potential energy is gradually transformed into electric energy. The situation of motor input does not affect the rotor speed owing to the mechanical switch being off. The input speed only affects the upward speed of the mass block. Therefore, the rotor always rotates at a steady speed, and the electric energy output by the G-TEG is steady. Fig. 5b–d shows the different stages when the input conditions are respectively a uniform speed, accelerated speed, and random speed. The speed returns to zero each time the motor speed changes. The revolution speed in Fig. 5b–d is thus not continuous. In Fig. 5e–g, the short-circuit currents correspond to the three input conditions, and all steady maximums of short-circuit currents under the three input conditions are almost 15 μA . Corresponding curves of the open-circuit voltage and the transferred charge are shown in Fig. S6 (Supporting Information).

2.4. Demonstration

A series of experiments, as presented in Fig. 6, were conducted to confirm that the designed G-TEG can harvest natural wind energy for practical applications. Fig. 6a shows the time taken for different commercial capacitors to charge from 0 to 5 V. Fig. 6b shows a diagram of the experimental system of the G-TEG supplying electric energy to a board of light emitting diodes (LEDs). Fig. 6c shows the random variation of the wind speed during the lighting of the LED board. The G-TEG successfully lights up the LED board continuously, such that there is steady brightness. The pictures in Fig. 6d compare the lighting when using the G-TEG and normal TENG. Details are presented in Supporting Movie S1. Fig. 6d corresponds to the time period of 43–45 s in Supporting Movie S1. Fig. 6e shows a capture of the G-TEG experiment conducted in a natural wind environment. It shows that the G-TEG can power a commercial thermometer in a natural wind environment, as

Table 1
Minimal values of I_{SD} and I_{FD} for the G-TEG.

	L_{ab-1}, M_1	L_{ab-2}, M_2	L_{ab-3}, M_3
I_{SD}	0.42 μA	0.31 μA	0.46 μA
I_{FD}	5.5%	2.3%	5.4%

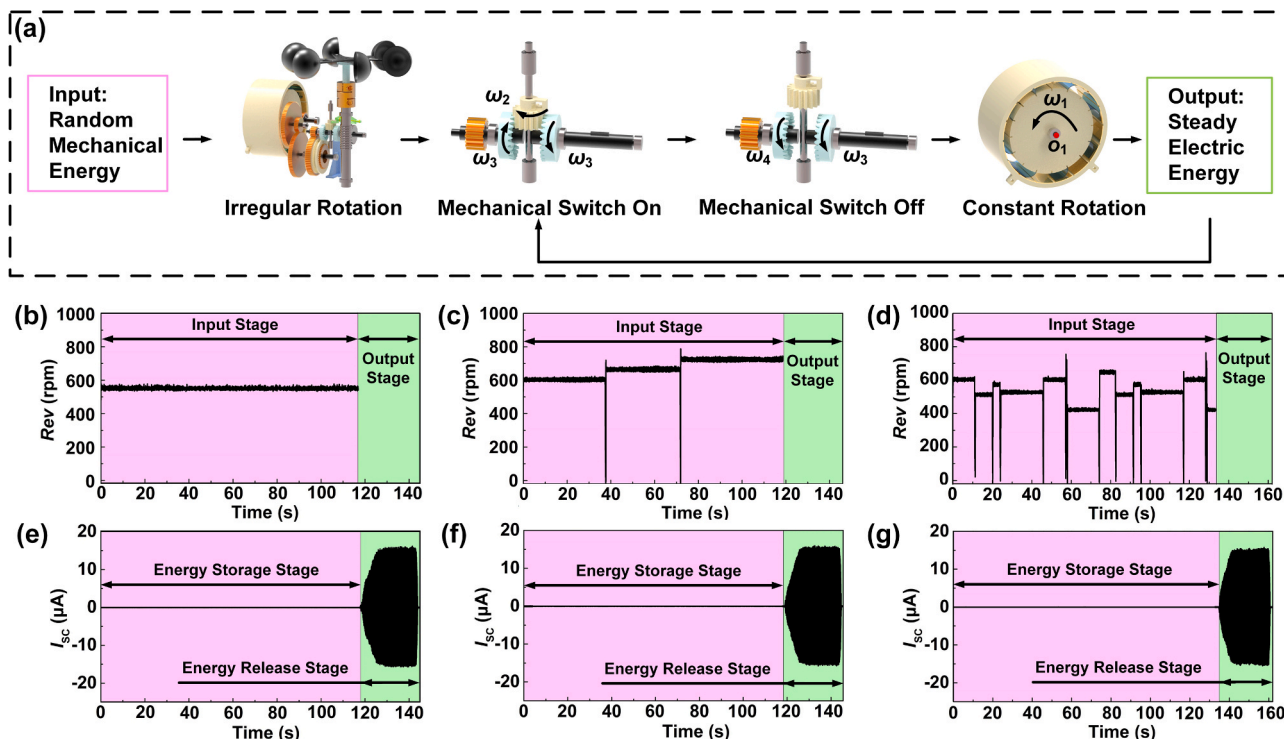


Fig. 5. (a) Experimental process of the G-TENG; the output performance of the G-TENG for different rotation inputs: (b, e) uniform rotating input, (c, f) accelerated rotating input, and (d, g) random rotating input.

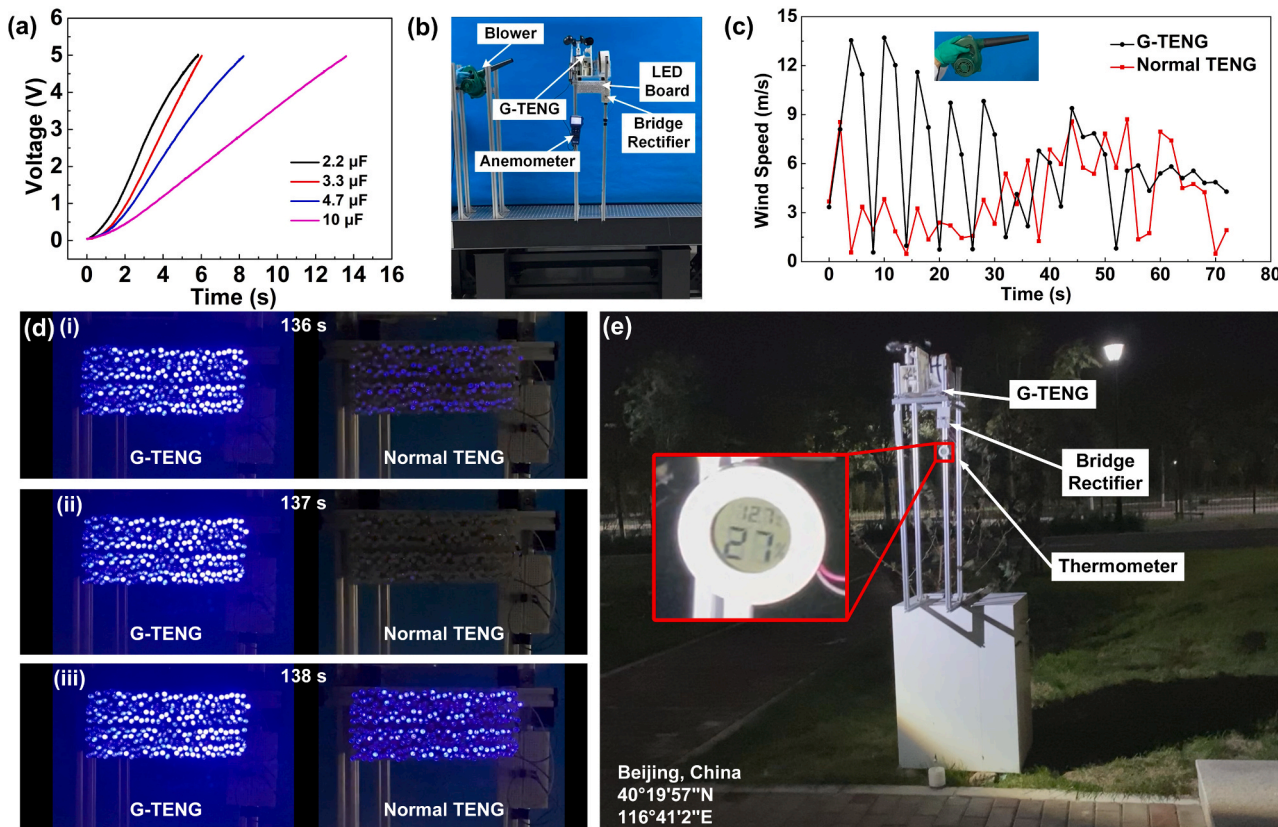


Fig. 6. Application of the G-TENG: (a) different commercial capacitors charged from 0 to 5 V, (b) experimental platform in the environment of a simulated wind, (c) wind speed curves when lighting an LED board, (d) comparison of performance in lighting an LED board using the G-TENG and normal TENG, and (e) capture of the G-TENG experiment conducted in a natural wind environment. Inset: enlarged view of the thermometer.

shown in Supporting Movie S2.

Supplementary material related to this article can be found online at [doi:10.1016/j.nanoen.2020.105740](https://doi.org/10.1016/j.nanoen.2020.105740).

3. Conclusions

In summary, a gravity triboelectric nanogenerator (G-TENG) is demonstrated to address the issue of the unsteady current output of a normal TENG. The proposed G-TENG comprises an energy input module, energy storage module, and energy output module. The G-TENG converts natural wind energy into gravitational potential energy, and steady electric energy is ultimately obtained. Therefore, a reliable method is provided in this research that the natural wind energy is converted into steady electric energy. The experimental results show that the standard deviation (I_{SD}) of short-circuit current peaks is under 0.31 μA , and the fluctuation degree (I_{FD}) reaches 2.3%. The G-TENG can supply electric energy for applications in a natural wind environment. This research provides significant guidance for generating steady electric energy and powering electronic devices.

4. Experimental section

4.1. Fabrication of the G-TENG

The gravity triboelectric nanogenerator (G-TENG) has dimensions of 70 mm (length) \times 80 mm (width) \times 220 mm (height). The shells of the G-TENG are fabricated by 3D printing and laser cutting, the printed material being polylactic acid (PLA), and the laser cutting material being acrylic. The gear-shifting unit of the G-TENG is machined using a lathe. The fluorinated ethylene propylene (FEP) film has a thickness of 100 μm and width of 50 mm. Sixteen copper electrodes with a thickness of 0.065 mm, width of 60 mm, and length of 20 mm are evenly distributed on the inner wall of the stator in the generation unit. Other information is given as [Supporting Information](#).

4.2. Electrical measurement

The rotation is generated by a stepper motor (J-5718HBS401, Yisheng, China) and the signal of G-TENG was captured by a programmable electrometer (6514, Keithley, USA) and a data acquisition system (PCI-6259, National Instruments, USA). The signal is transmitted to the computer and recorded by LabVIEW.

CRedit authorship contribution statement

Yuqi Wang: Conceptualization, Investigation, Writing - original draft. **Xin Yu:** Investigation, Writing - original draft. **Mengfei Yin:** Investigation, Validation. **Jianlong Wang:** Investigation. **Qi Gao:** Investigation. **Yang Yu:** Investigation. **Tinghai Cheng:** Conceptualization, Resources, Writing - review & editing, Supervision. **Zhong Lin Wang:** Conceptualization, Resources, Writing - review & editing, Supervision.

Declaration of Competing Interest

The authors declare that they have no known competing financial interests or personal relationships that could have appeared to influence the work reported in this paper.

Acknowledgments

The authors are grateful for the supports received from the National Key R&D Project from the National Key R & D Project from Minister of Science and Technology (2016YFA0202704), the Beijing Municipal Science and Technology Commission (Z171100002017017), and National Natural Science Foundation of China (51775130).

Appendix A. Supporting information

Supplementary data associated with this article can be found in the online version at [doi:10.1016/j.nanoen.2020.105740](https://doi.org/10.1016/j.nanoen.2020.105740).

References

- [1] Z.L. Wang, Triboelectric nanogenerators as new energy technology for self-powered systems and as active mechanical and chemical sensors, *ACS Nano* 7 (2013) 9533–9557.
- [2] Z.L. Wang, W.Z. Wu, Nanotechnology-enabled energy harvesting for self-powered micro-/nanosystems, *Angew. Chem. Int. Ed.* 51 (2012) 11700–11721.
- [3] Z.L. Wang, On Maxwell's displacement current for energy and sensors: the origin of nanogenerators, *Mater. Today* 20 (2017) 74–82.
- [4] Z.L. Wang, A.C. Wang, On the origin of contact-electrification, *Mater. Today* 30 (2019) 34–51.
- [5] Z.L. Wang, Triboelectric nanogenerators as new energy technology and self-powered sensors - principles, problems and perspectives, *Faraday Discuss.* 176 (2014) 447–458.
- [6] J.X. Zhu, M.L. Zhu, Q.F. Shi, F. Wen, L. Liu, B.W. Dong, A. Haroun, Y.Q. Yang, P. Vachon, X.G. Guo, T.Y.Y. He, C.K. Lee, Progress in TENG technology—a journey from energy harvesting to nanoenergy and nanosystem, *EcoMat* (2020) 1–45, <https://doi.org/10.1002/eom2.12058>.
- [7] H.C. Liu, H.L. Fu, L.N. Sun, C.K. Lee, E.M. Yeatman, Hybrid energy harvesting technology: from materials, structural design, system integration to applications, *Renew. Sustain. Energy Rev.* (2020), 110473, <https://doi.org/10.1016/j.rser.2020.110473>.
- [8] F.-R. Fan, Z.-Q. Tian, Z.L. Wang, Flexible triboelectric generator, *Nano Energy* 1 (2012) 328–334.
- [9] J.W. Zhong, Q.Z. Zhong, F.-R. Fan, Y. Zhang, S.H. Wang, B. Hu, Z.L. Wang, J. Zhou, Finger typing driven triboelectric nanogenerator and its use for instantaneously lighting up LEDs, *Nano Energy* 2 (2013) 491–497.
- [10] Q. Tang, M.-H. Yeh, G.L. Liu, S.M. Li, J. Chen, Y. Bai, L. Feng, M.H. Lai, K.-C. Ho, H. Y. Guo, C.G. Hu, Whirligig-inspired triboelectric nanogenerator with ultrahigh specific output as reliable portable instant power supply for personal health monitoring devices, *Nano Energy* 47 (2018) 74–80.
- [11] P.H. Wang, L. Pan, J.Y. Wang, M.Y. Xu, G.Z. Dai, H.Y. Zou, K. Dong, Z.L. Wang, An ultra-low-friction triboelectric-electromagnetic hybrid nanogenerator for rotation energy harvesting and self-powered wind speed sensor, *ACS Nano* 12 (2018) 9433–9440.
- [12] I.-W. Tcho, S.-B. Jeon, S.-J. Park, W.-G. Kim, I.K. Jin, J.-K. Han, D. Kim, Y.-K. Choi, Disk-based triboelectric nanogenerator operated by rotational force converted from linear force by a gear system, *Nano Energy* 50 (2018) 489–496.
- [13] G. Zhu, Y. Yang, S.H. Wang, C.F. Pan, Z.L. Wang, Progress in nanogenerators for portable electronics, *Mater. Today* 15 (2012) 532–543.
- [14] Z.M. Lin, B.B. Zhang, H.Y. Guo, Z.Y. Wu, H.Y. Zou, J. Yang, Z.L. Wang, Super-robust and frequency-multiplied triboelectric nanogenerator for efficient harvesting water and wind energy, *Nano Energy* 64 (2019), 103908.
- [15] G.L. Liu, H.Y. Guo, S.X. Xu, C.G. Hu, Z.L. Wang, Oblate spheroidal triboelectric nanogenerator for all-weather blue energy harvesting, *Adv. Energy Mater.* 9 (2019), 1900801.
- [16] X.D. Yang, L. Xu, P. Lin, W. Zhong, Y. Bai, J.J. Luo, J. Chen, Z.L. Wang, Macroscopic self-assembly network of encapsulated high-performance triboelectric nanogenerators for water wave energy harvesting, *Nano Energy* 60 (2019) 404–412.
- [17] W. Zhong, L. Xu, X.D. Yang, W. Tang, J.J. Shao, B.D. Chen, Z.L. Wang, Open-book-like triboelectric nanogenerators based on low-frequency roll-swing oscillators for wave energy harvesting, *Nanoscale* 11 (2019) 7199–7208.
- [18] J. Chen, G. Zhu, W.Q. Yang, Q.S. Jing, P. Bai, Y. Yang, T.-C. Hou, Z.L. Wang, Harmonic-resonator-based triboelectric nanogenerator as a sustainable power source and a self-powered active vibration sensor, *Adv. Mater.* 25 (2013) 6094–6099.
- [19] H.S. Wang, C.K. Jeong, M.-H. Seo, D.J. Joe, J.H. Han, J.-B. Yoon, K.J. Lee, Performance-enhanced triboelectric nanogenerator enabled by wafer-scale nanogrates of multistep pattern downscaling, *Nano Energy* 35 (2017) 415–423.
- [20] H.F. Zhao, X. Xiao, P. Xu, T.C. Zhao, L.G. Song, X.X. Pan, J.C. Mi, M.Y. Xu, Z. L. Wang, Dual-tube helmholtz resonator-based triboelectric nanogenerator for highly efficient harvesting of acoustic energy, *Adv. Energy Mater.* 9 (2019), 1902824.
- [21] F.-R. Fan, J.J. Luo, W. Tang, C.Y. Li, C.Q. Zhang, Z.Q. Tian, Z.L. Wang, Highly transparent and flexible triboelectric nanogenerators: performance improvements and fundamental mechanisms, *J. Mater. Chem. A* 2 (2014) 13219–13225.
- [22] W. Seung, H.-J. Yoon, T.Y. Kim, H. Ryu, J. Kim, J.-H. Lee, J.H. Lee, S. Kim, Y. K. Park, Y.J. Park, S.-W. Kim, Boosting power-generating performance of triboelectric nanogenerators via artificial control of ferroelectric polarization and dielectric properties, *Adv. Energy Mater.* 7 (2017), 1600988.
- [23] Z.W. Ren, Z.M. Wang, Z.R. Liu, L.F. Wang, H.Y. Guo, L.L. Li, S.T. Li, X.Y. Chen, W. Tang, Z.L. Wang, Energy harvesting from breeze wind (0.7–6 m s^{-1}) using ultra-stretchable triboelectric nanogenerator, *Adv. Energy Mater.* 10 (2020), 2001770.
- [24] M. Jošt, B. Lipovšek, B. Glazar, A. Al-Ashouri, K. Brecl, G. Matic, A. Magomedov, V. Getautis, M. Topić, S. Albrecht, Perovskite solar cells go outdoors: field testing and temperature effects on energy yield, *Adv. Energy Mater.* 10 (2020), 2000454.

- [25] M.-L. Seol, J.-H. Woo, S.-B. Jeon, D. Kim, S.-J. Park, J. Hur, Y.-K. Choi, Vertically stacked thin triboelectric nanogenerator for wind energy harvesting, *Nano Energy* 14 (2015) 201–208.
- [26] K.Q. Xia, J.M. Fu, Z.W. Xu, Multiple-frequency high-output triboelectric nanogenerator based on a water balloon for all-weather water wave energy harvesting, *Adv. Energy Mater.* 10 (2020), 2000426.
- [27] L. Xu, Y.K. Pang, C. Zhang, T. Jiang, X.Y. Chen, J.J. Luo, W. Tang, X. Cao, Z. L. Wang, Integrated triboelectric nanogenerator array based on air-driven membrane structures for water wave energy harvesting, *Nano Energy* 31 (2017) 351–358.
- [28] T.H. Cheng, Y.K. Li, Y.-C. Wang, Q. Gao, T. Ma, Z.L. Wang, Triboelectric nanogenerator by integrating a cam and a movable frame for ambient mechanical energy harvesting, *Nano Energy* 60 (2019) 137–143.
- [29] Q. Gao, Y.K. Li, Z.J. Xie, W.X. Yang, Z. Wang, M.F. Yin, X.H. Lu, T.H. Cheng, Z. L. Wang, Robust triboelectric nanogenerator with ratchet-like wheel-based design for harvesting of environmental energy, *Adv. Mater. Technol.* 5 (2019), 1900801.
- [30] M.F. Yin, Y. Yu, Y.Q. Wang, Z. Wang, X.H. Lu, T.H. Cheng, Z.L. Wang, Multi-plate structured triboelectric nanogenerator based on cycloidal displacement for harvesting hydroenergy, *Extrem. Mech. Lett.* 33 (2019), 100576.
- [31] W.X. Yang, Y. Wang, Y.K. Li, J.L. Wang, T.H. Cheng, Z.L. Wang, Integrated flywheel and spiral spring triboelectric nanogenerator for improving energy harvesting of intermittent excitations/triggering, *Nano Energy* 66 (2019), 104104.
- [32] X.H. Lu, Y.H. Xu, G.D. Qiao, Q. Gao, X.S. Zhang, T.H. Cheng, Z.L. Wang, Triboelectric nanogenerator for entire stroke energy harvesting with bidirectional gear transmission, *Nano Energy* 72 (2020), 104726.
- [33] M.F. Yin, X.H. Lu, G.D. Qiao, Y.H. Xu, Y.Q. Wang, T.H. Cheng, Z.L. Wang, Mechanical regulation triboelectric nanogenerator with controllable output performance for random energy harvesting, *Adv. Energy Mater.* 10 (2020), 2000627.
- [34] W.X. Yang, Q. Gao, X. Xia, X.S. Zhang, X.H. Lu, S.T. Yang, T.H. Cheng, Z.L. Wang, Travel switch integrated mechanical regulation triboelectric nanogenerator with linear–rotational motion transformation mechanism, *Extrem. Mech. Lett.* 37 (2020), 100718.